IEEE Access
Multidisciplinary | Rapid Review | Open Access Journal

Received May 8, 2020, accepted May 22, 2020, date of publication June 2, 2020, date of current version June 16, 2020.

Digital Object Identifier 10.1109/ACCESS.2020.2999344

Analysis of Traveling Strategies for Driving Omni-Wheeled Vehicle Around a Corner

SIYING LONG, TATSURO TERAKAWA, MASAHARU KOMORI, (Member, IEEE), AND TAKUMI OUGINO

Department of Mechanical Engineering and Science, Kyoto University, Kyoto 6158540, Japan

Corresponding author: Tatsuro Terakawa (terakawa@me.kyoto-u.ac.jp)

ABSTRACT Vehicles equipped with omnidirectional wheels can move in any direction, which means that many driving strategies are available, even for a simple task like turning a corner. However, the characteristics of each driving strategy have not yet been explored to detect what kind of strategy is suitable for what path conditions for what reasons. This study aims to clarify and compare the phenomena that occur in the possible least-time driving strategies for an omni-wheeled vehicle while it turns a corner. Three traveling strategies are proposed according to the order of rotation and turning motion, for which the possible least-time patterns are presented. Simulations are conducted to analyze the advantages of each pattern and compare the three traveling strategies for various path and corner configurations. The results show that the strategy in which the vehicle rotates during or after turning motion costs the least time. When both the path width and corner angle are small, the vehicle should turn with a large radius to maintain a high velocity. In contrast, the vehicle should turn with a small radius when the corner angle is large, even if this requires deceleration.

INDEX TERMS Vehicle, omni wheel, traveling strategy, time cost, corner.

I. INTRODUCTION

Transportation vehicles are widely used in warehouses and factories to deliver materials or components to a target location. Most of these vehicles use conventional wheels, such as tired wheels, for their simplicity and high reliability. However, such conventional wheeled vehicles have a disadvantage in mobility. Specifically, they can only move forward and backward or steer toward the required direction, but they cannot move laterally and diagonally, which may make it difficult for the vehicles to move, especially in a narrow passage.

Vehicles equipped with omnidirectional wheels, which can immediately move in an arbitrary direction, including the right, left, or diagonal direction, have the potential to solve the problem of limited mobility [1], [2]. Vehicles with omnidirectional wheels can move efficiently even in a limited space compared with vehicles with conventional wheels [3]–[5]. Several types of mechanisms have been studied to form omnidirectional wheels. A major example is the omni wheel, which has a series of free rollers along the outer circumference of the wheel main body, as shown in Fig. 1. When the wheel main body is driven by a motor, the wheel rotates actively in one direction. When the free rollers are rotated by an external force, the wheel runs passively in another direction. Their combination allows the vehicle with three or more omni wheels to move in an arbitrary direction [6], [7]. An omni wheel with actively driven rollers can realize omnidirectional movement even with two wheels [8]–[10]. As another example, the Mecanum wheel has several free rollers attached to the circumference of the wheel main body at an angle [11]–[13]. The Mecanum wheel can move in a similar way to the omni wheel. The spherical wheel is a ball-shaped wheel that is driven by multiple rollers or wheels [14]–[16]. By the combination of the rollers or wheels driven by motors, the spherical wheel can move actively in any direction.

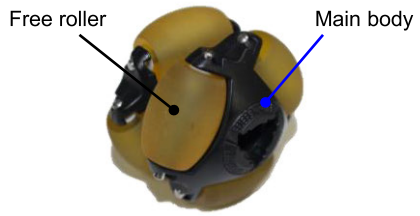

FIGURE 1. Omni wheel.

There have been studies not only on the motion analysis and modeling of the omnidirectional vehicles but also on their

The associate editor coordinating the review of this manuscript and approving it for publication was Hamid Mohammad-Sedighi.

motion planning. Various approaches concerning the motion planning were proposed, such as the dynamic inversion-based scheme for the real-time trajectory generation [17], the global path planning system composed of the odometry, motion controller, and global path planner [18], and the local reactive approach for avoiding the moving obstacles [19]. These studies aim to search for the time-optimal trajectory when vehicles with omnidirectional mobility need to avoid obstacles. The specific algorithm makes it possible to find out optimal traveling trajectory according to boundary conditions. However, it has not been fully explored what kind of strategy is advantageous in what circumstances for what reasons. An omnidirectional wheeled vehicle can move forward/backward, to the left/right, and rotate. Therefore, various driving strategies are possible even for a simple task, such as turning a corner. It is interesting to clarify the characteristics of each driving strategy for the omnidirectional wheeled vehicle systematically and show what kind of driving strategy is suitable for each situation.

Based on these points, the present study aims to reveal the features of the driving strategies for an omnidirectional wheeled vehicle by comparing the fundamental driving strategies when the vehicle goes through a specified area to offer a reference for finding the most time-efficient motion. This paper discusses a vehicle equipped with the omni wheels having passive rollers. A simple kinetic model with nonslip conditions of the omni-wheeled vehicle (OWV) was constructed to implement simulations. The specified traveling area comprised two sets of intersecting straight lines to form a corner with various angles. The possible traveling strategies were proposed according to the path conditions. The features of these motion strategies were analyzed through simulations when the path conditions vary.

II. MODELING OF OWV AND DEFINITION OF TRAVELING AREA

This section describes the OWV kinetic model and defines the traveling area. Because this study focused on discussing and comparing the fundamental characteristics of traveling strategies, a simplified situation is considered. The driving motors were assumed to be ideal. In other words, the motor torque is large enough to rotate the wheels without delay, including at high speed. In addition, the maximum driving force of each wheel is considered to be equal to the maximum static friction force between the wheel and ground regardless of the rotation speed of the wheel.

A. KINETIC MODEL OF OWV

The OWV model shown in Fig. 2(a) consists of a square body and four omni wheels arranged at the center of each side in parallel. The distance between opposite wheels is d. The center of gravity is on the vertical axis passing through the center of the body and does not move relative to the vehicle while the vehicle moving. Each wheel is driven independently and can output driving force in one direction. A coordinate system x_o-y_o is fixed at the center of the vehicle, and its x_o and y_o axes run parallel to the diagonal lines of the body, as shown in Fig. 2(a).

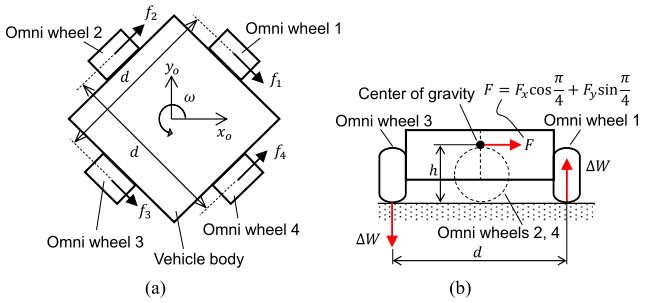

FIGURE 2. Omni-wheeled vehicle (OWV) model. (a) Top view of OWV. (b) Load transfer between omni wheels 1 and 3.

The equations of motion can be calculated as

$$\begin{cases} m\dot{v}_x = F_x = \dfrac{1}{\sqrt{2}}\left(f_1 + f_2 + f_3 + f_4\right) \\ m\dot{v}_y = F_y = \dfrac{1}{\sqrt{2}}\left(-f_1 + f_2 - f_3 + f_4\right) \\ I\dot{\omega} = T_r = \dfrac{d}{2}\left(-f_1 - f_2 + f_3 + f_4\right) \end{cases} \tag{1}$$

where $f_i (i = 1, 2, 3, 4)$ is the driving force of omni wheel i; v_x and v_y are the velocities in the x_o-axis and y_o-axis directions, respectively; ω is the rotation velocity; F_x and F_y are the driving force of the vehicle in the x_o-axis and y_o-axis directions, respectively; T_r is rotation torque; m is the mass of the OWV; and I is the moment of inertia.

Next, we consider the nonslip condition for the OWV. The load on each omni wheel is $mg/4$ when the vehicle is in a static state. However, the load will transfer because of the inertial force while the vehicle is accelerating [20]. When the amount of the load transfer between omni wheels 1 and 3 is set as ΔW, as shown in Fig. 2(b), it can be calculated with consideration of the equilibrium of the moment.

$$d\Delta W = h(F_x \cos\frac{\pi}{4} + F_y \sin\frac{\pi}{4}) \tag{2}$$

Therefore, $\Delta W = h\left(F_x + F_y\right)/\left(\sqrt{2}d\right)$ is given, where h is the height of the center of gravity from the floor. The load transfer between omni wheels 2 and 4 is given in the same way. As a result, the nonslip condition for each wheel is written as

$$\begin{cases} |f_1|/\mu \le \dfrac{mg}{4} - \dfrac{h}{\sqrt{2}d}\left(F_x + F_y\right) \\ |f_2|/\mu \le \dfrac{mg}{4} + \dfrac{h}{\sqrt{2}d}\left(F_x - F_y\right) \\ |f_3|/\mu \le \dfrac{mg}{4} + \dfrac{h}{\sqrt{2}d}\left(F_x + F_y\right) \\ |f_4|/\mu \le \dfrac{mg}{4} - \dfrac{h}{\sqrt{2}d}\left(F_x - F_y\right). \end{cases} \tag{3}$$

B. DEFINITION OF TRAVELING AREA

In the practical use of transportation vehicles, the area where the vehicle can move is usually limited because of obstacles

or surrounding constructions. Thus, we strictly defined the area in which the vehicle can move. This paper focuses on an angled path with one corner as the most fundamental situation because many different environments can be described by combining angled paths. Fig. 3 shows the target traveling area, where the x-y coordinate system is placed on the ground. Both edges of the area are straight lines. The position of the vehicle is represented by the center of gravity and the vehicle is constrained to keep its center of gravity within the area while moving. The intersection point of the centerlines is set as reference point O. The initial and terminal points are M and N, respectively. The path width is D and the corner angle is θ, which is set as $0 < \theta \leq \pi/2$ with the consideration of symmetry. The distances from point M to O (first half path) and that from point O to N (second half path) are defined as l_1 and l_2, respectively. The point at which the inner angles intersect, that is the inside of the corner, is set as point P.

The motion of the vehicle running through the traveling area is divided into two types: linear motion with uniform acceleration and turning of the corner. First, the vehicle starts moving at point M with the velocity $v_m = 0$ and accelerates along the centerline of the path using linear motion. When approaching the corner, the vehicle transits to turning motion. After passing through the corner, the vehicle resumes linear motion. The start and end points of turning are set as S and F, respectively. The distances between point S and O and between point O and F are set as l_s and l_f, respectively. The direction of the velocity vector at point S and F is parallel to the path edges. Velocities at point S and F are set as v_s and v_f, respectively. The time cost for the first linear motion, turning of the corner, and second linear motion are set as t_{ms}, t_{sf} and t_{fn}, respectively. The summed time cost T is used to assess the entire motion.

$$T = t_{ms} + t_{sf} + t_{fn}. \tag{4}$$

In addition, we required the OWV to return to the centerline after turning. Thus, the velocity direction at point F is coincident with the centerline. The vehicle can choose to rotate clockwise or counterclockwise to adjust its heading to the velocity direction, which is determined according to the time cost.

III. OWV DRIVING STRATEGY

This section discusses the possible traveling strategies of OWV within the defined area. The traveling direction of the conventional vehicle is fixed relative to the vehicle body, but OWV can move in any direction. According to (1) and (3), the driving force of the OWV should satisfy the following equation:

$$|F_x| + |F_y| \leq \frac{\mu mg}{\sqrt{2}}. \tag{5}$$

Therefore, the maximum value of the driving force varies depending on the direction, as shown in Fig. 4. The driving force takes the largest value on the boundaries of a quadrangular area. The four boundaries are called modes I, II, III, and IV.

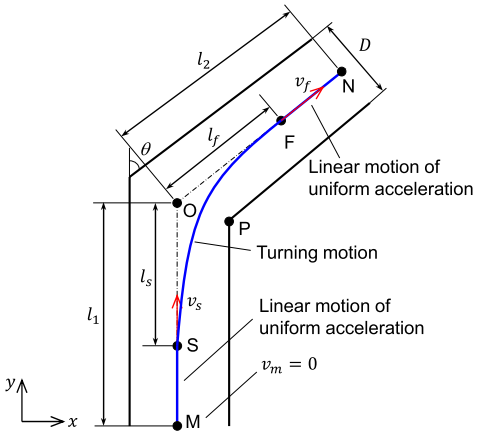

FIGURE 3. Definition of traveling area and its parameters.

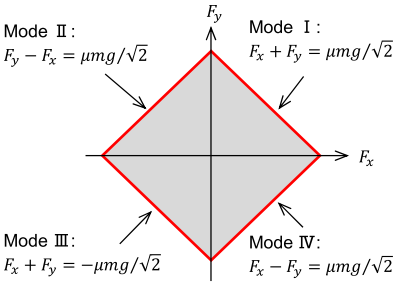

FIGURE 4. Distribution of driving force in the x_o-y_o coordinate system.

The OWV can perform turning, during which the vehicle travels with a changing velocity vector, and rotation, during which the vehicle changes its orientation with respect to the traveling direction. The order and timing of these motions, which are performed independently, determine the traveling strategy. Here, three forms of traveling strategies are considered according to the order of the above motions as follows:

Form A: Changing the vehicle orientation after changing the velocity vector direction, namely, rotation after turning.

Form B: Changing the velocity vector direction after changing the orientation, namely, rotation before turning.

Form C: Changing the vehicle orientation and velocity vector direction at the same time, namely, rotation during turning.

The kinetic model of each form is discussed in the following sections.

A. FORM A: ROTATION AFTER TURNING

Without the restriction of the traveling area, the acceleration during the first linear motion and during the turning motion should take the maximum value to reduce the time cost, which can be calculated as

$$\begin{cases} |\dot{v}_y| = \dfrac{\mu g}{\sqrt{2}}, \dot{v}_x = 0 & \text{for the first linear motion} \\ |\dot{v}_x| = \dfrac{\mu g}{\sqrt{2}}, \dot{v}_y = 0 & \text{for the turning motion.} \end{cases} \tag{6}$$

After turning, the vehicle can accelerate and rotate either independently or at the same time. Therefore, there are three possible operating modes: rotation before acceleration, rotation after acceleration, and rotation during acceleration. When the vehicle rotates and accelerates independently, assuming that the translational acceleration is zero and the rotation torque takes the maximum value during rotation, the time cost of the rotation t_r can be calculated by the following equation:

$$\begin{cases} I\dfrac{d\omega}{dt} = \dfrac{1}{2}\mu mgd \\ \min\left(\theta, \dfrac{\pi}{2} - \theta\right) = \omega t_r. \end{cases} \tag{7}$$

As a result, the equations of motion for independent acceleration and rotation can be written as

$$\begin{cases} v_f t_r + v_f\left(t_{fn} - t_r\right) + \dfrac{\mu g}{2\sqrt{2}}\left(t_{fn} - t_r\right)^2 = l_2 - l_f \\ \uparrow \text{ for acceleration after rotation} \\ v_f\left(t_{fn} - t_r\right) + \dfrac{\mu g\left(t_{fn} - t_r\right)^2}{2\sqrt{2}\left(\cos\theta + \sin\theta\right)} \\ \quad + \left[v_f + \dfrac{\mu g(t_{fn} - t_r)}{\sqrt{2}(\cos\theta + \sin\theta)}\right] t_r = l_2 - l_f \\ \uparrow \text{ for rotation after acceleration.} \end{cases} \tag{8}$$

When the vehicle accelerates and rotates at the same time, there is a trade-off between rotation torque and translational driving force. We focus on the situation where the angular velocity at both points F and N is zero, the angular acceleration is distributed symmetrically between the first and second halves, and the driving force takes the maximum value that satisfies the nonslip condition. The equations of motion are given as follows:

$$\begin{cases} I\dot{\omega} = T_{r1}, \dfrac{1}{2}\dot{\omega}t_h^2 = \dfrac{\beta}{2} \quad \text{for } 0 \le \varphi \le \dfrac{\beta}{2} \\ I\dot{\omega} = T_{r2}, \dot{\omega}t_h\left(t_{fn} - t_h\right) + \dfrac{1}{2}\dot{\omega}\left(t_{fn} - t_h\right) = \dfrac{\beta}{2} \\ \quad \text{for } \dfrac{\beta}{2} < \varphi \le \beta \\ \displaystyle\int_0^{t_{fn}/2}\int \frac{F_{t1}}{m}dvdt + \int_{t_{fn}/2}^{t_{fn}}\int \frac{F_{t2}}{m}dvdt = l_2 - l_f \\ F_{t1}, F_{t2} = \max\left(F_x\sin(\theta - \varphi) + F_y\cos(\theta - \varphi)\right) \\ \quad \text{if } 0 \le \theta \le \pi/4 \\ F_{t1}, F_{t2} = \max\left(F_x\sin(\theta + \varphi) + F_y\cos(\theta + \varphi)\right) \\ \quad \text{if } \pi/4 < \theta \le \pi/2 \\ t_{fn} = 2t_h, T_{r1} = -T_{r2}, \beta = \min\left(\theta, \dfrac{\pi}{2} - \theta\right) \end{cases} \tag{9}$$

where T_{r1} and T_{r2} are the driving torques of the first and second halves of the rotation, respectively; F_{t1} and F_{t2} are the driving force of the first and second halves of the translation, respectively; t_h is the time cost of the first half of the rotation; and φ is the rotation angle of the vehicle body. We can obtain t_{fn} with the combination of (1), (3), and (9).

Of these three forms, the one that has the smallest time cost is chosen as the motion after turning. The resulting motion is defined as pattern A0.

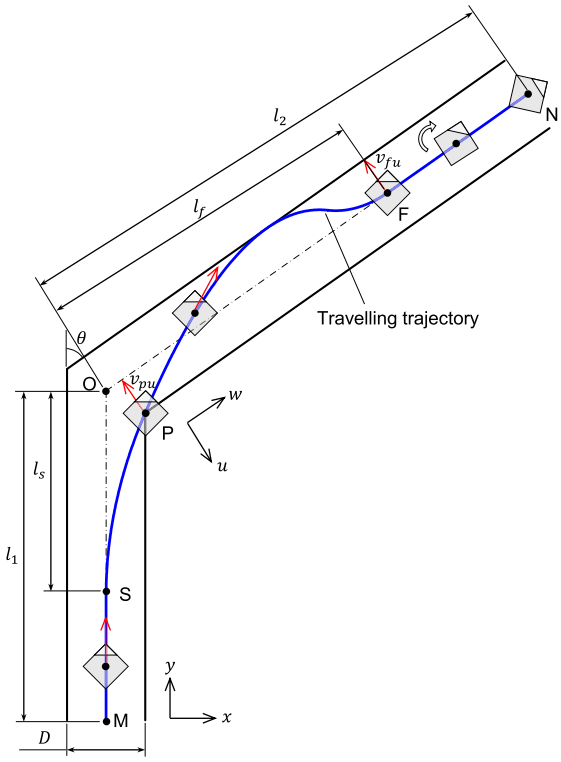

FIGURE 5. Motion trajectory of form A.

When taking the restriction of the traveling area into account, the strategy discussed above can be the optimal motion if there is no deviation from the traveling area. Otherwise, the vehicle should decelerate in the y-axis direction before turning. However, the OWV can accelerate in the x-axis direction and decelerate in the y-axis direction at the same time. To use the path width maximally, the trajectory should pass through point P. Then, the time cost from point S to point P t_{sp} can be calculated by the following equation:

$$\begin{cases} F_x - F_y = \dfrac{\mu mg}{\sqrt{2}} \\ \dfrac{1}{2}\dfrac{F_x}{m}t_{sp}^2 = \dfrac{D}{2} \\ v_s t_{sp} - \dfrac{1}{2}\dfrac{F_y}{m}t_{sp}^2 = l_s - \dfrac{D}{2}\tan\dfrac{\theta}{2} \end{cases} \tag{10}$$

where l_s is a variable whose suitable value will be determined to minimize the time cost.

Here, the u-w coordinate system shown in Fig. 5 is employed to discuss the movement after point P conveniently. The u and w axes are perpendicular and parallel to the second half of the path, respectively. The velocity in the u-axis direction at point P v_{pu} must be negative to avoid the departure from the path.

The driving force relation is translated from the x-y coordinate system to the u-w coordinate system as shown in Fig. 6. The driving forces in the u-axis and w-axis directions are set as F_u and F_w, respectively. When $0 < \theta \le \pi/4$, it is inferred from Fig. 6(a) that mode I is the most suitable because both F_u and F_w can take large values. In this situation, the acceleration

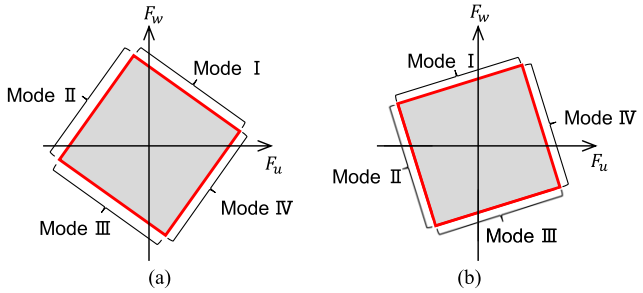

FIGURE 6. Distribution of driving force in *u-w* coordinate system. (a) $0 < \theta \le \pi/4$, and (b) $\pi/4 < \theta \le \pi/2$.

in the u-axis direction should lie within the following range:

$$-\frac{\mu g \sin\theta}{\sqrt{2}} \le \ddot{u} \le \frac{\mu g \cos\theta}{\sqrt{2}}. \tag{11}$$

It is necessary to make the velocity in the u-axis direction at point F, v_{fu}, equal to zero. When the trajectory of the vehicle converges with the centerline, the relation of the acceleration and velocity between point P and F can be obtained as follows:

$$v_{pu}t_{pf} - \frac{\ddot{u}t_{pf}^2}{2} \le \frac{D}{2} \wedge v_{fu} = v_{pu} - \ddot{u}t_{pf} = 0 \Leftrightarrow \ddot{u} \ge \frac{v_{pu}^2}{D} \tag{12}$$

where t_{pf} is the time cost between points P and F. As a result, when $v_{pu}^2/D \le \mu g \cos\theta/\sqrt{2}$, the acceleration should be set as $\ddot{u} = -\mu g \sin\theta/\sqrt{2}$ to let the vehicle travel toward the centerline from the inner edge and then change to $\ddot{u} = \mu g \cos\theta/\sqrt{2}$ to let the vehicle converge with the centerline. This series of motions is defined as pattern A1.

When v_{pu} is too large to make the trajectory converge with the centerline, the vehicle should travel toward the outer edge within the limitation of the path width.

$$\begin{aligned} v_{pu}t_{po} - \frac{\ddot{u}t_{po}^2}{2} \le D \wedge v_{ou} = v_{pu} - \ddot{u}t_{po} = 0 \wedge t_{pf} \\ = t_{po} + t_{of} \Leftrightarrow \ddot{u} \ge \frac{v_{pu}^2}{2D} \end{aligned} \tag{13}$$

where t_{po} is the time cost from point P to the point nearest to the outer edge, t_{of} is the time cost from that point to point F, and v_{ou} is the velocity in the u-axis direction at that point. In summary, when $v_{pu}^2/D > \mu g \cos\theta/\sqrt{2}$, the acceleration should be set as $\ddot{u} = \mu g \cos\theta/\sqrt{2}$ to let the vehicle cross the centerline to the outer edge and then change to $\ddot{u} = -\mu g \sin\theta/\sqrt{2}$ to let the vehicle converge with the centerline. These series of motions are defined as pattern A2.

When $\pi/4 < \theta \le \pi/2$, Fig. 6(b) shows that F_u in mode IV is larger than that in mode I. As a result, it is necessary to use mode IV with mode I in some cases. In this situation, the acceleration in the u-axis direction should lie within the following range:

$$-\frac{\mu g \sin\theta}{\sqrt{2}} \le \ddot{u} \le \frac{\mu g \sin\theta}{2}. \tag{14}$$

The basic idea to finish the path is the same as when using only mode I, as described above. When using mode IV, the traveling patterns are defined as patterns A3, A4, and A5. Pattern A3 aims at turning the corner without crossing the centerline under the condition $v_{pu}^2/D \le \mu g \sin\theta/\sqrt{2}$. When the vehicle cannot travel by pattern A3, that is, when $v_{pu}^2/D > \mu g \sin\theta/\sqrt{2}$, the vehicle is permitted to cross the centerline in pattern A4. When $v_{pu}^2/2D > \mu g \cos\theta/\sqrt{2}$, the vehicle travels to touch the outer edge so that the deceleration in the u-axis direction is minimized, which is defined as pattern A5.

The trajectories of patterns A0-A5 from point P are shown in Fig. 7. The flowchart of determining the optimal motion for the traveling strategy of form A is shown in Fig. 8.

B. FORM B: ROTATION BEFORE TURNING

When traveling with the traveling strategy of form B, the OWV first rotates, which changes the vehicle's orientation to direct the front toward the w-axis direction, and then turns, as shown in Fig. 9.

Without the restriction of the traveling area, assuming that rotational torque takes the maximum value and the translational velocity stays constant during the rotation, the equations of motion can be written as follows:

$$\begin{cases} \frac{1}{2}\dot{v}_y (t_{ms} - t_r)^2 + v_s t_r = l_1 - l_s, \dot{v}_y = \frac{\mu g}{\sqrt{2}}, \dot{v}_x = 0 \\ \uparrow \text{ for motion before rotation} \\ I\frac{d\omega}{dt} = \frac{1}{2}\mu mgd, \min\left(\theta, \frac{\pi}{2} - \theta\right) = \omega t_r \\ \uparrow \text{ for motion during rotation} \\ v_s \sin\theta = \ddot{u}t_{sf}, \ddot{u} = \frac{\mu g}{\sqrt{2}}, \ddot{w} = 0 \\ \uparrow \text{ for motion during turning.} \end{cases} \tag{15}$$

The strategy for the turning motion is the same as that in form A. In the second linear motion, the vehicle travels straight at the maximum acceleration. The above series of motions are defined as pattern B0.

When the restriction of the traveling area is taken into account, the trajectory should pass through point P to obtain the maximal turning radius. Therefore, the equation of motion from point S to point P is as follows:

$$\begin{cases} F_x - F_y = \frac{\mu mg}{\sqrt{2}} \\ \frac{1}{2}\frac{F_x}{m}t_{sp}^2 = \frac{D}{2} \\ v_s t_{sp} - \frac{1}{2}\frac{F_y}{m}t_{sp}^2 = l_s - \frac{D}{2}\tan\frac{\theta}{2} - v_s t_r. \end{cases} \tag{16}$$

A suitable value of l_s will be determined to minimize the time cost.

After passing through point P, acceleration in the w-axis direction should be positive. Fig. 10 shows the driving force relation in the u-w coordinate system when $\theta > \pi/4$. According to Fig. 10, modes I and IV are suitable because the value of F_w stays positive. When a combination of modes I and IV is used, the boundary of acceleration in the u-axis direction is given as follows:

$$-\frac{\mu g}{\sqrt{2}} \le \ddot{u} \le \frac{\mu g}{\sqrt{2}}. \tag{17}$$

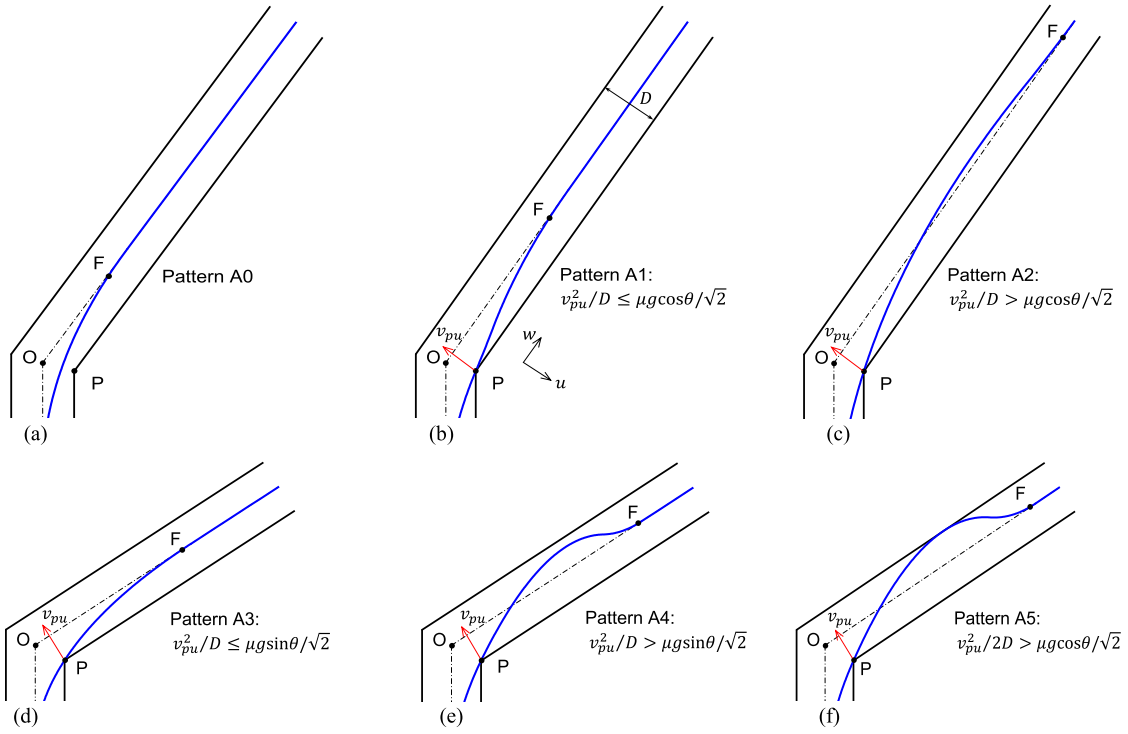

FIGURE 7. Traveling patterns of form A. (a) Pattern A0, (b) Pattern A1, (c) Pattern A2, (d) Pattern A3, (e) Pattern A4 and (f) Pattern A5.

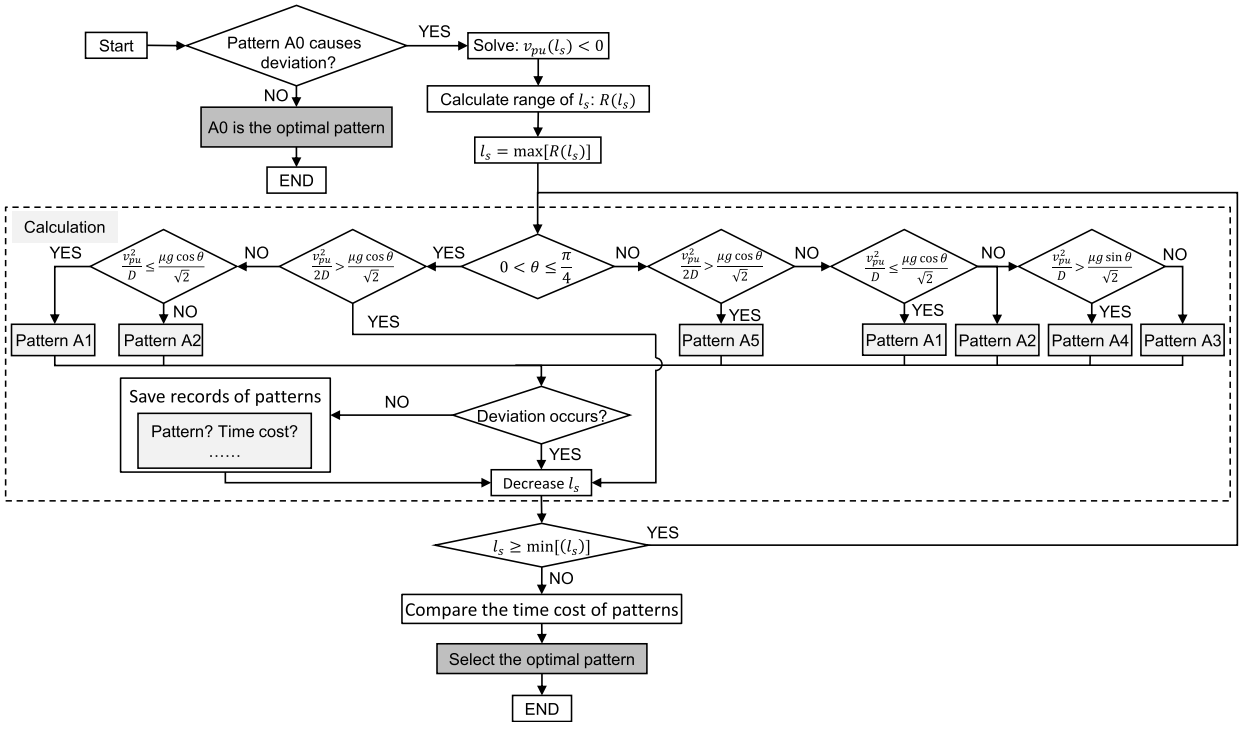

FIGURE 8. Flowchart of determining optimal motion for form A.

When $\theta \le \pi/4$, modes I and II instead of modes I and IV should be chosen, but the strategy is the same.

It is also necessary for the vehicle to converge with the centerline as quickly as possible, namely, to minimize l_f to gain the space needed to accelerate during the second linear motion. The conditions of (17) allow three patterns of motion: B1, B2, and B3. In the case of $v_{pu}^2/D \le \mu g/\sqrt{2}$, the vehicle simply approaches the centerline, which is defined as pattern B1. When v_{pu} is larger, that is, $\mu g/\sqrt{2} < v_{pu}^2/D \le \sqrt{2}\mu g$, the vehicle crosses the centerline, which is defined as pattern B2.

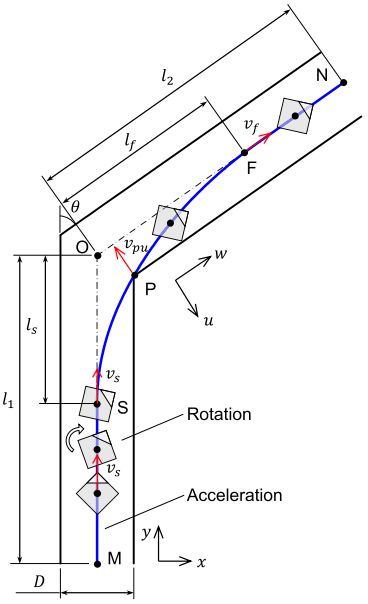

FIGURE 9. Motion trajectory of form B.

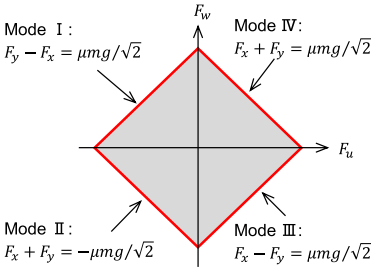

FIGURE 10. Distribution of driving force for form B in u-w coordinate system when $\theta > \pi/4$.

When the width of the path is so limited that $v_{pu}^2/D > \sqrt{2}\mu g$ is satisfied, the vehicle can travel only if it touches the outer edge of the path, which is pattern B3.

The trajectories of patterns B0-B3 from point P are shown in Fig. 11. The flowchart of determining the optimal pattern for the traveling strategy of form B is shown in Fig. 12.

C. FORM C: ROTATION DURING TURNING

In the traveling strategy of form C, the vehicle rotates and turns at the same time. In the first and second linear motions, the vehicle can run with the maximum acceleration $\mu g/\sqrt{2}$. According to (1) and (2), the rotational angular acceleration during turning can be calculated as follows:

$$\begin{cases} \dfrac{d}{2I}\left(-\mu mg + \sqrt{2}mv\omega\right) \le \dot{\omega} \le \dfrac{d}{2I}\left(\mu mg - \sqrt{2}mv\omega\right) \\ \quad \text{if } \omega \ge 0 \\ \dfrac{d}{2I}\left(-\mu mg - \sqrt{2}mv\omega\right) \le \dot{\omega} \le \dfrac{d}{2I}\left(\mu mg + \sqrt{2}mv\omega\right) \\ \quad \text{if } \omega < 0. \end{cases} \tag{18}$$

When the restriction of the traveling area is not considered, the summary time cost of finishing the path is minimized if the acceleration of the linear motion and turning motion takes the maximum values. At this time, the linear acceleration is equal to $\sqrt{2}\mu g/2$, while the angular acceleration is as

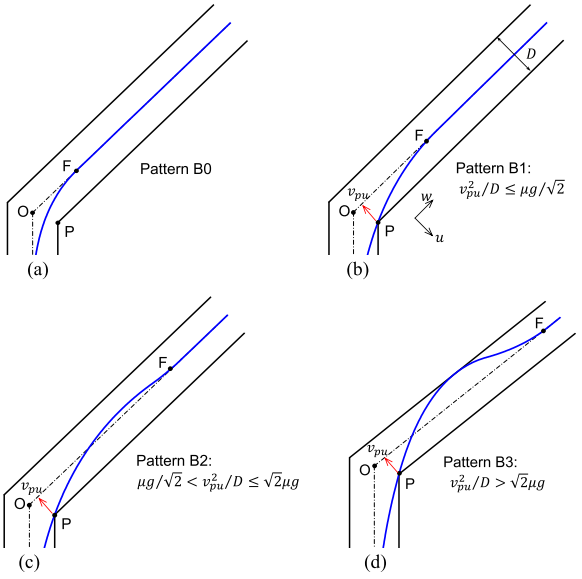

FIGURE 11. Motion patterns of form B. (a) Pattern B0, (b) Pattern B1, (c) Pattern B2 and (d) Pattern B3.

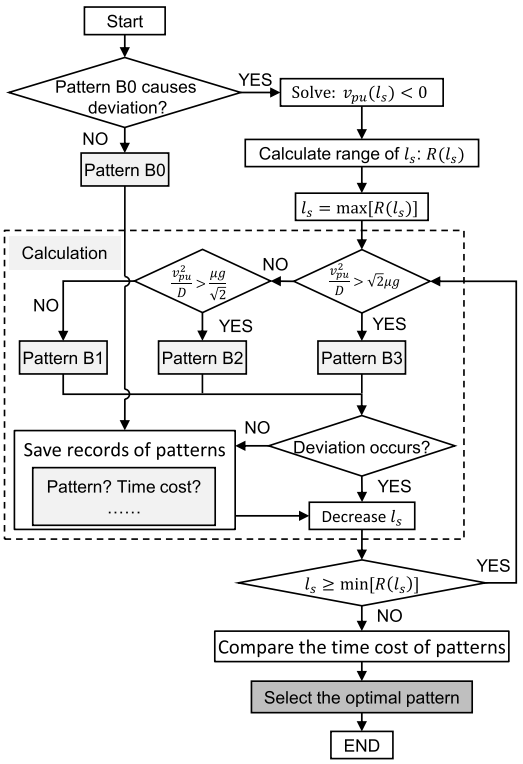

FIGURE 12. Flowchart of determining optimal motion for form B.

follows:

$$\dot{\omega} = \begin{cases} \dfrac{d}{2I}\left(-\mu mg - \sqrt{2}mv\omega\right) & \text{for } 0 \le \displaystyle\int (-\omega)\, dt \le \frac{\theta}{2} \\ \dfrac{d}{2I}\left(\mu mg + \sqrt{2}mv\omega\right) & \text{for } \dfrac{\theta}{2} < \displaystyle\int (-\omega)\, dt \le \theta. \end{cases} \tag{19}$$

This style of motion is defined as pattern C0.

The limited width of the path may cause the vehicle to deviate from the traveling area during turning. To avoid

TABLE 1. Traveling patterns of OWV from point P with respect to route centerline.

Form	Pattern	Trajectory of pattern	Form	Pattern	Trajectory of pattern
Form A (rotation after turning)	A0	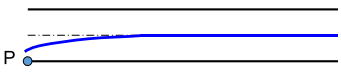	Form B (rotation before turning)	B0	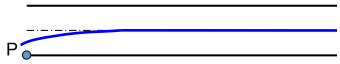
	A1			B1	
	A2	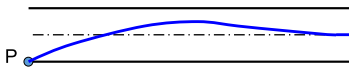		B2	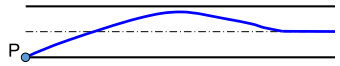
	A3	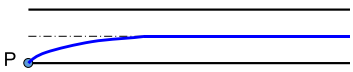		B3	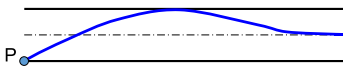
	A4	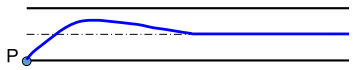	Form C (rotation during turning)	C0	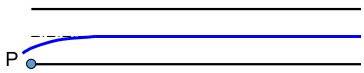
	A5	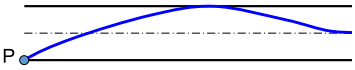		C1	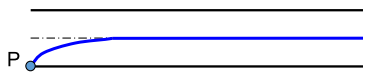
				C2	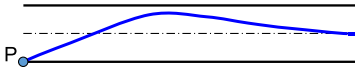

this, deceleration before turning is necessary, similar to that needed in forms A and B. In this case, there are two motion patterns depending on whether the vehicle is permitted to cross the centerline or not, which are defined as patterns C1 and C2, respectively. The trajectories of patterns C0-C2 are shown in Fig. 13.

All motion patterns for the traveling strategy of forms A, B, and C are summarized in Table 1.

IV. ANALYSIS AND COMPARISON OF THREE TRAVELING STRATEGIES

The proposed traveling strategies are analyzed and compared through simulations in this section. The parameters of OWV used in the simulation are listed in Table 2.

A. CHARACTERISTICS OF FORM A

First, we discuss the characteristics of the trajectories in the six motion patterns for form A. Fig. 14 shows examples of the trajectories calculated under the condition of $l_1 = l_2 = 10$ m. The figure shows that the variation of the corner angle θ and path width D affects the pattern features. The trajectories cut off in the middle indicate that a deviation occurs at that point. In pattern A0, where the vehicle runs at the largest acceleration without considering the restriction of the traveling area, the vehicle can stay on the path only when θ is small and D is large [Fig. 14(a)]. Comparison of patterns A1 and A2 shows that, although their trajectories are similar to each other in Fig. 14(b), the trajectory crosses the centerline in pattern A2 but not in pattern A1, as shown in Fig. 14(c), (d), and (e). The trajectory of pattern A2 has the advantage of less deceleration before turning the corner, but

TABLE 2. Simulation parameters of OWV.

Symbol	Description
m	3.0 kg
g	9.8 m/s^2
d	0.3 m
h	0.15 m
μ	0.3
I	0.045 kg·m^2

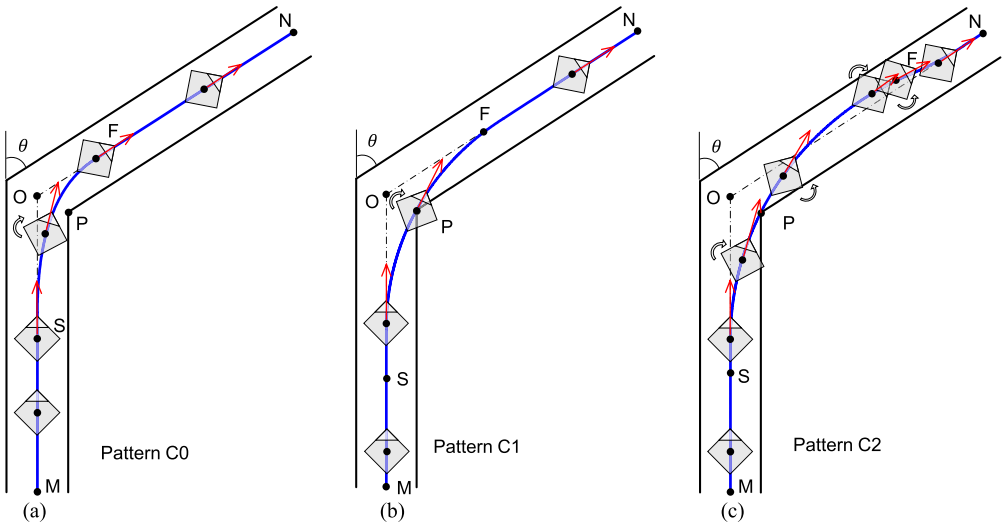

FIGURE 13. Traveling approach of form C. (a) Pattern C0, (b) Pattern C1, and (c) Pattern C2.

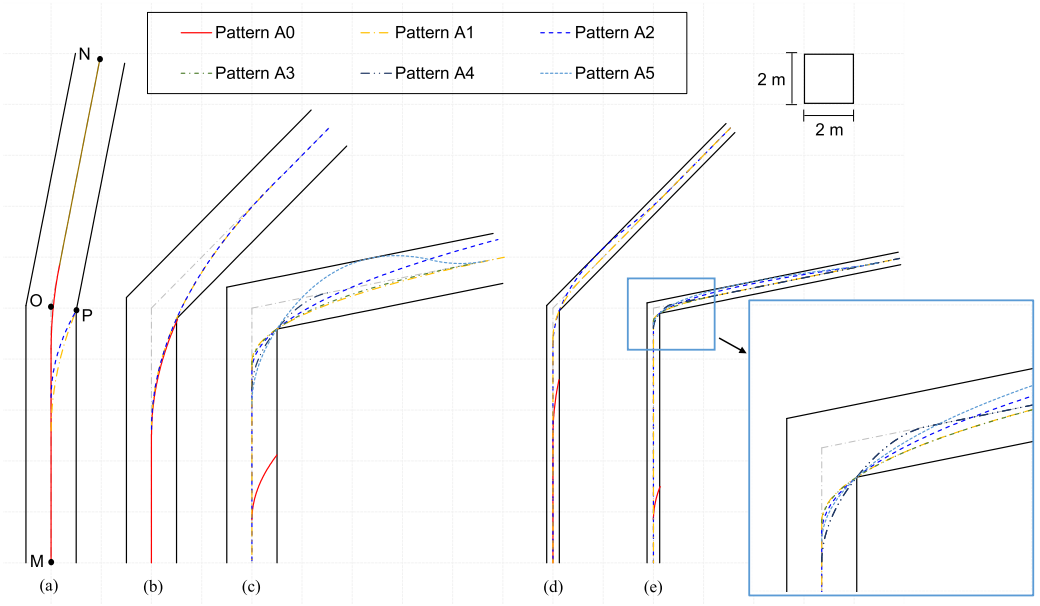

FIGURE 14. Trajectories of six motion patterns of form A with $l_1 = 10$ m and $l_2 = 10$ m. (a) $D = 2.0$ m, $\theta = \pi/16$ (b) $D = 2.0$ m, $\theta = 4\pi/16$ (c) $D = 2.0$ m, $\theta = 7\pi/16$ (d) $D = 0.5$ m, $\theta = 4\pi/16$ (e) $D = 0.5$ m, $\theta = 7\pi/16$.

at the same time it has the disadvantage of a larger travel distance. Pattern A1 has the opposite effects. For patterns A3, A4, and A5, their trajectories reach the centerline after turning in the order of A4, A3, and A5 in both Fig. 14(c) and (e). This means that the trajectory of pattern A4 goes over the centerline slightly and the trajectory of A5 travels well past the centerline, while pattern A3 establishes a track somewhere in the middle without crossing over the centerline. With respect to D, a narrow path makes turning the corner difficult in general, but it contributes to decreased travel distance in patterns A2 and A5, as shown by comparing Fig. 14(c) and (e).

Next, the traveling time cost is compared according to the variation of the path conditions. Fig. 15 shows the calculation results of the least-time cost when the corner angle θ varies with $l_2 = 10$ m and $D = 2.0$ m. The name of the least-time pattern is shown beside each sampling point. In the graph, as θ becomes larger, the time cost tends to increase and the optimal patterns change. When θ is small, the vehicle can travel by pattern A0 and the time cost increases only a little.

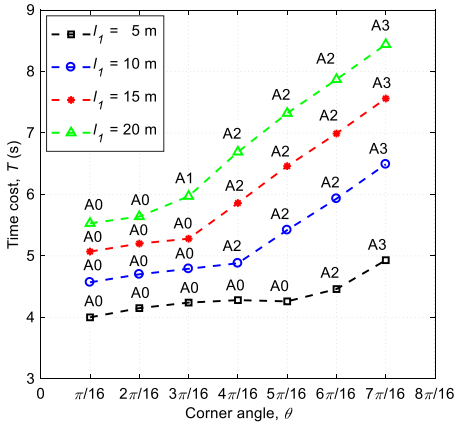

FIGURE 15. Least-time cost of form A when corner angle varies with $l_2 = 10$ m and $D = 2.0$ m.

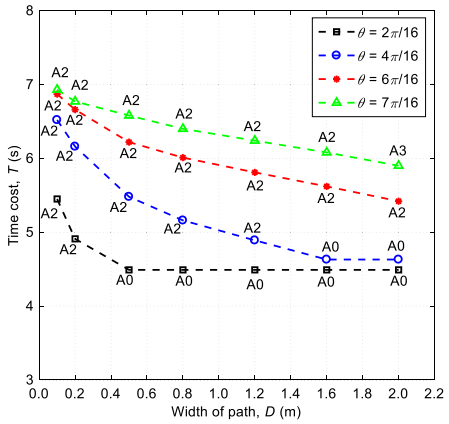

FIGURE 16. Least-time cost of form A when path width varies with $l_1 = 8.0$ m and $l_2 = 10$ m.

Then, after pattern A0 is no longer feasible due to the large θ, the optimal pattern switches to pattern A2 and finally A3. At this point, the time cost shows stronger growth because the OWV must decelerate before turning. When l_1 is large enough, for example, $l_1 = 20$ m, pattern A1 also appears between A0 and A2.

Fig. 16 shows the time cost when the width of the path D varies with $l_1 = 8.0$ m and $l_2 = 10$ m. The graph shows that the time cost tends to decrease as D increases and that the least-time pattern changes due to the variation and consequently converges to pattern A0. Once pattern A0 becomes feasible, the time cost remains constant even when D changes. When D is relatively small, the time cost decreases strongly, for the same reasons seen in Fig. 15.

By expanding the calculation results, we explored the driving strategy according to various configurations of the traveling area. Fig. 17 shows the regions of the least-time patterns when the corner angle θ and the first half path length l_1 are varied with $l_2 = 10$ m and $D = 2.0$ m. When θ or l_1 is relatively small, the vehicle can always travel with pattern A0, so that pattern A0 should be chosen. However, when θ and l_1 become larger, pattern A0 is no longer feasible because of the limited path width and then pattern A1 or A2 takes its

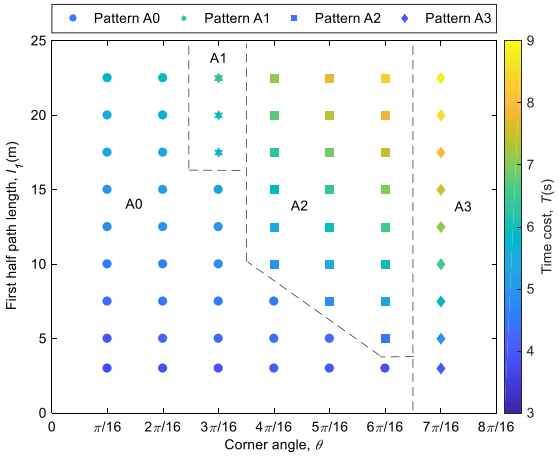

FIGURE 17. Distribution of least-time patterns of form A with $l_2 = 10$ m and $D = 2.0$ m.

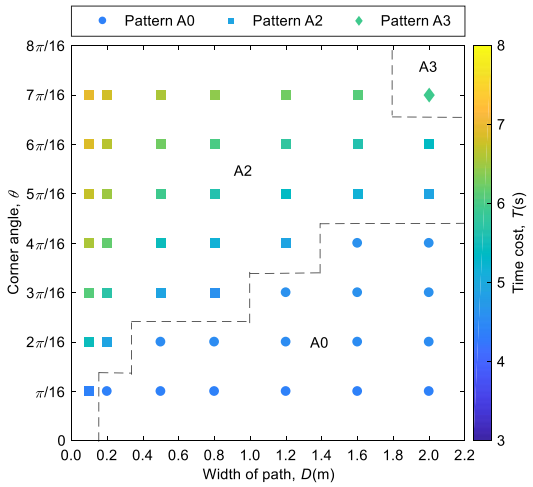

FIGURE 18. Distribution of least-time patterns of form A with $l_1 = 8.0$ m and $l_2 = 10$ m.

place. The trajectories of patterns A1 and A2 are close to each other under the specific corner angle, for example, $\theta = \pi/4$ shown in Fig. 14(b). When θ becomes larger, in other words, when the corner angle is severe, pattern A2 is advantageous because its trajectory can obtain a large turning radius, which contributes to minimizing deceleration. In contrast, pattern A1 is faster than pattern A2 when θ is smaller because it has a sufficiently large turning radius without crossing the centerline. When θ is still larger, that is, $\theta = 7\pi/16$, it becomes difficult for the vehicle to return to the centerline quickly after turning the corner in pattern A2. That leads to an increase in the moving distance and time cost. In this case, pattern A3, which draws a turning radius larger than the radius of pattern A4 and smaller in length than that of pattern A5, becomes the fastest.

Fig. 18 shows the distribution of the least-time patterns when D and θ are varied with $l_1 = 8.0$ m and $l_2 = 10$ m. As shown in the graph, pattern A0 is feasible when D is large enough with reference to θ. Otherwise, it is basically advantageous for the vehicle to travel by pattern A2, as shown

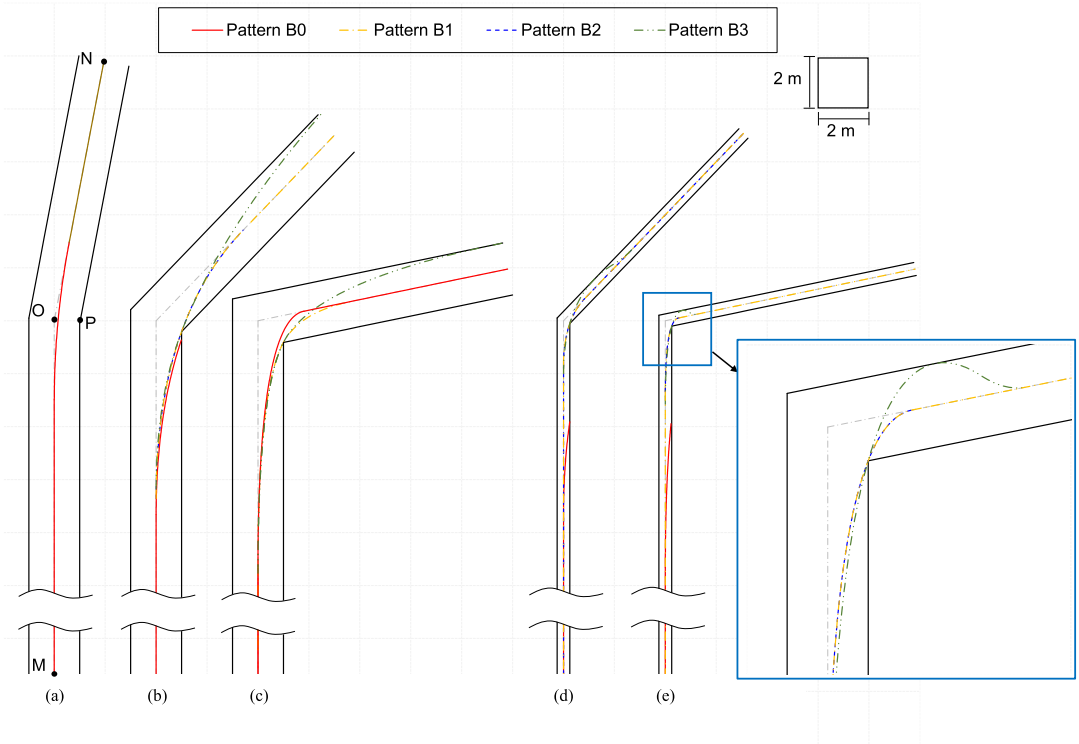

FIGURE 19. Trajectories of form B when $l_1 = 20$m and $l_2 = 10$ m. (a) $D = 2.0$ m, $\theta = \pi/16$ (b) $D = 2.0$ m, $\theta = 4\pi/16$ (c) $D = 2.0$ m, $\theta = 7\pi/16$ (d) $D = 0.5$ m, $\theta = 4\pi/16$ (e) $D = 0.5$ m, $\theta = 7\pi/16$.

in Fig. 17. In contrast to the distribution shown in Fig. 17, pattern A2 has superiority even when θ is large and D is small in Fig. 18. This might be because a small D minimizes the divergence of the trajectory from the centerline, and then the traveling distance is decreased. Consequently, pattern A3 becomes the fastest when D is large at the same time that θ approaches $\pi/2$.

In summary, the optimal pattern A0 is feasible when θ or l_1 is small and D is large. Otherwise, pattern A2 is the next best candidate. As an exception, pattern A3 is quickest when θ approaches $\pi/2$ and D is large, and pattern A1 is quickest when l_1 is large and θ is somewhat small.

B. CHARACTERISTICS OF FORM B

Fig. 19 shows the trajectories for form B with $l_1 = 20$ m and $l_2 = 10$ m. The trajectory of pattern B0 deviates from the path when its width is small [Fig. 19(d) and (e)]. In contrast, when the path is relatively wide, the trajectory deviates only when the corner angle is around $\pi/4$ [Fig. 19(b)], whereas no deviation occurs when the corner angle is smaller or larger than $\pi/4$ [Fig. 19(a) and (c)]. Before point P, the vehicle has to decelerate in the y-axis direction and accelerate in the x-axis direction. Therefore, when the corner angle is large, the acceleration in the x-axis direction becomes large relative to the deceleration in the y-axis direction, and this causes a deviation. When the corner angle is still larger, however, the vehicle accelerates in the x-axis direction slowly because the driving force is almost entirely consumed by the deceleration in the y-axis direction. As a result, the turning maneuver proceeds gradually and the trajectory can avoid deviation from the path.

In these conditions, the trajectory of patterns B1 and B2 are close to each other. It should be noted that the trajectory of pattern B1 is shorter than that of pattern B0 when the corner angle is somewhat large as shown in [Fig. 19(c)], which suggests the possibility for pattern B1 to perform better than pattern B0 in form B. Pattern B3 fails to converge to the centerline when the path width is large [Fig. 19(b) and (c)]. In contrast, the trajectory stays within the path when its width is small [Fig. 19(d) and (e)]. Note that the trajectories that are not shown in the figure, specifically, patterns B1–B3 in Fig. 19(a) and pattern B2 in Fig. 19(c), do not have a solution.

Here the calculation results are used to discuss the choice of motion patterns. Fig. 20 shows the distribution of the least-time patterns of form B when the corner angle θ and the first-half path length l_1 vary with $l_2 = 10$ m and $D = 2.0$ m. Here, pattern B0 costs the least time in most cases. However, when l_1 increases, pattern B0 deviates from the path around $\theta = \pi/4$, as shown in Fig. 19(b). In this case, pattern B1 becomes the least-time pattern instead of pattern B0. When l_1 becomes even larger, pattern B2 costs less time than the others. This is thought to be because a larger l_1 increases the initial velocity and consequently requires larger deceleration before turning in pattern B1.

Fig. 21 shows the distribution of the least-time patterns when D and θ vary with $l_1 = 8.0$ m and $l_2 = 10$ m. Basically, the time cost of pattern B0 is lower than that of the others when D is sufficiently large. However, when D

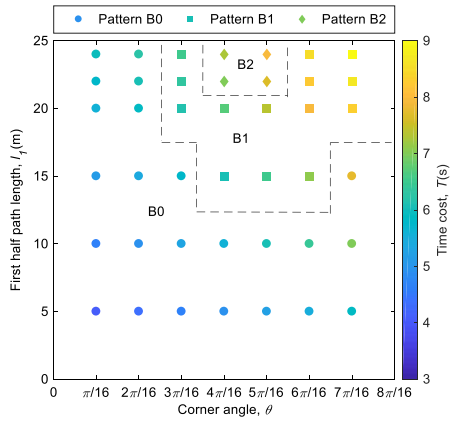

FIGURE 20. Distribution of least-time patterns of form B with $l_2 = 10$ m and $D = 2.0$ m.

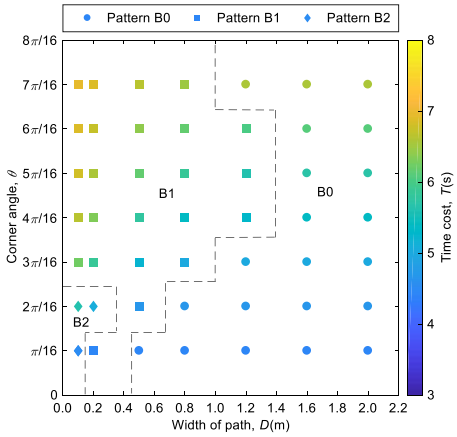

FIGURE 21. Distribution of least-time patterns of form B with $l_1 = 8.0$ m and $l_2 = 10$ m.

becomes small, pattern B1 costs the least because the trajectory of pattern B0 leaves the path. Pattern B0 becomes disadvantageous especially when θ approaches $\pi/4$, which is the same result shown in Fig. 20. Conversely, when D is small, pattern B2 has the lowest time cost because the effect of the longer moving distance stays relatively small. However, when θ increases under small D, most of the driving force is consumed to adjust the velocity in the u-axis direction in pattern B2, so that pattern B1 becomes the least-time pattern.

In summary, pattern B0 is feasible except around $\theta = \pi/4$ when D is large and l_1 is not. In other cases, pattern B1 has the lowest time cost. When l_1 is large or θ and D are small, pattern B2 shows its advantage.

C. CHARACTERISTICS OF FORM C

Fig. 22 shows some trajectories for form C with $l_1 = l_2 = 10$ m. The trajectory of pattern C0 deviates from the path when the corner angle is large [Fig. 22(c)] or the path is narrow [Fig. 22(d) and (e)]. Comparison of patterns C1 and C2 show that the trajectory of pattern C1 converges to the centerline quickly, while the trajectory of pattern C2 needs to cross the centerline once. This suggests that pattern C1 has an advantageously short trajectory. In contrast, the trajectory of pattern C2 has a large turning radius, which allows the vehicle to run at a high velocity. Note that the trajectory of pattern C1 is not shown in Fig. 22(a) and (b) and that of pattern C2 is not shown in Fig. 22(a) because they do not have solutions. Pattern C2 fails to reach the centerline at $\theta = \pi/4$, as shown in Fig. 22(b).

Fig. 23 shows the distribution of the least-time patterns when the corner angle θ and the first half path length l_1 vary with $D = 2.0$ m and $l_2 = 10$ m. Pattern C0 has the lowest time cost when l_1 or θ is small. When l_1 and θ becomes larger, pattern C0 is no longer feasible due to deviation from the path. In this situation, when θ is moderate, pattern C2 is advantageous because its trajectory can use a large turning radius, which contributes to keeping the velocity high. Conversely, when θ becomes still larger, the trajectory length of pattern C2 becomes long enough to offset the advantage of the higher velocity. At this time, pattern C1 has a better strategy due to its moving distance superiority.

Fig. 24 indicates the distribution of the least-time patterns when the path width D and the corner angle θ vary with $l_1 = 8.0$ m and $l_2 = 10$ m. Basically, traveling by pattern C0 has the lowest time cost when θ is relatively small and D is relatively large. In the other regions, pattern C1 or C2 is best. Compared to pattern C1, pattern C2 has an advantage with respect to velocity but a disadvantage with respect to traveling distance, as described above. When D is small, however, its disadvantage is minimized. Therefore, pattern C2 becomes the time-optimal pattern when both D and θ are relatively small. As D and θ increase, pattern C1 becomes superior.

In summary, we can use pattern C0 with the least-time cost when θ or l_1 is small and D is large. Otherwise, pattern C1 is advantageous when θ is large, whereas pattern C2 should be chosen when D is small.

D. COMPARISON OF FORMS A, B, AND C

Here, the results in the previous sections are compared to analyze the characteristics of the three traveling strategies. As explained above, the corner angle θ, the path width D, and the first and second half path lengths l_1 and l_2 affect the choice of patterns. Therefore, we compare the least-time cost to figure out what strategy is suitable for what situations when these parameters are varied.

First, the effect of the corner angle θ on the choice among the three traveling strategies is discussed. As shown in Fig. 25, form B always costs more time than forms A and C. This is partly because the rotation before turning in form B reduces the acceleration time and force in the first linear motion. Another reason is the direction of acceleration. In the situation of turning a corner whose angle is α, as shown in Fig. 26, in form B the vehicle velocity v becomes lower after turning than the velocity before turning v_s, while it becomes higher in form A and remains unchanged in form C. Specifically, this effect becomes more pronounced as the corner angle increases, which is thought to be the reason why the difference in the time cost between form B and the others

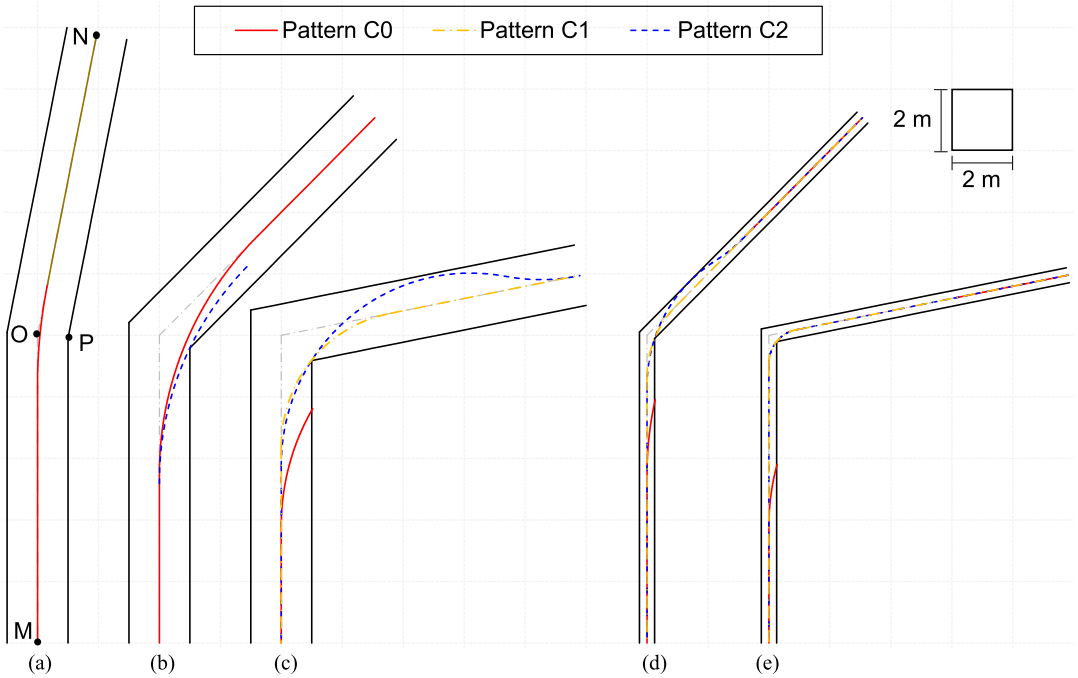

FIGURE 22. Traveling patterns of form C with $l_1 = 10$ *m*, $l_2 = 10$ m. (a) $D = 2.0$ m, $\theta = \pi/16$ (b) $D = 2.0$ m, $\theta = 4\pi/16$ (c) $D = 2.0$ m, $\theta = 7\pi/16$ (d) $D = 0.5$ m, $\theta = 4\pi/16$ (e) $D = 0.5$ m, $\theta = 7\pi/16$.

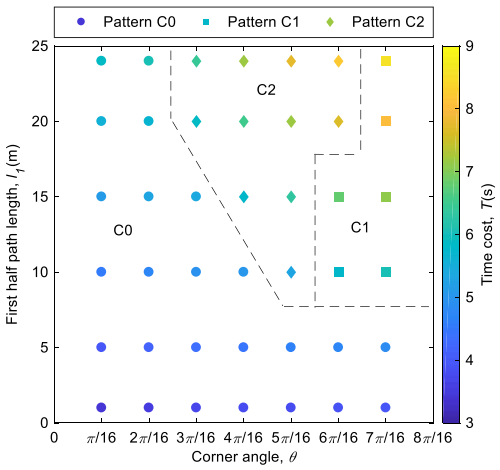

FIGURE 23. Distribution of least-time patterns of form C with $l_2 = 10$ m and $D = 2.0$ m.

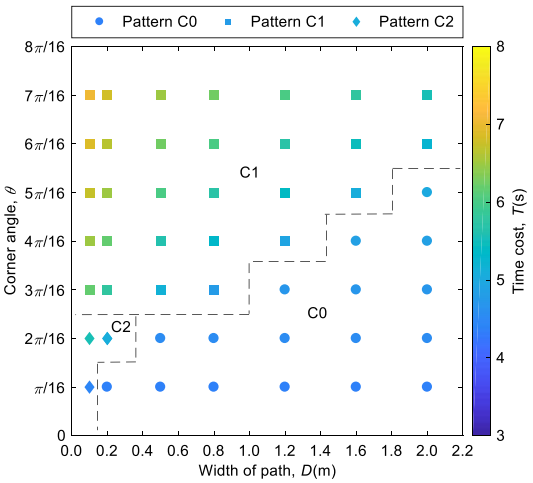

FIGURE 24. Distribution of least-time patterns of form C with $l_1 = 8.0$ m and $l_2 = 10$ m.

becomes larger when θ increases. Thus, form B is generally slower than forms A and C.

However, as shown in Fig. 25(a) and (b), when the second half path length l_2 is small, forms A and C cannot accomplish the travel under some conditions. The smaller value of l_2 made the vehicle unable to finish the rotation after or during turning by the proposed motion patterns. In the graph, this effect becomes more conspicuous when the first half path length l_1 increases, because this leads to a larger velocity during the turn. Therefore, sufficient deceleration before turning may contribute to completion of the trajectory, but the time cost increases. Compared with forms A and C, in form B, where the vehicle adjusts its orientation before turning the corner, the vehicle can avoid the deviation efficiently even under the severe conditions of limited l_2.

As shown in Fig. 25(a) and (c), form A is advantageous when l_1 is small. A smaller l_1 means reduced velocity during turning, which helps the motion patterns of form A to show their superiority without concern for deviation from the path. Additionally, form A becomes more advantageous when l_2 is sufficiently large, as shown in Fig. 25(c), because deviation is avoided. Form A shows the same tendency in Fig. 25(c) as in Fig. 15 at $l_1 = 5.0$ m. A smaller l_1 allows form A to travel by pattern A0 even in the severe corner of $\theta = 6\pi/16$. The time cost has a local maximum value at $\theta = \pi/4$ because the rotation angle of the vehicle becomes the largest at $\theta = \pi/4$ whether the vehicle rotates clockwise or counterclockwise. However, when θ becomes larger, the time cost increases

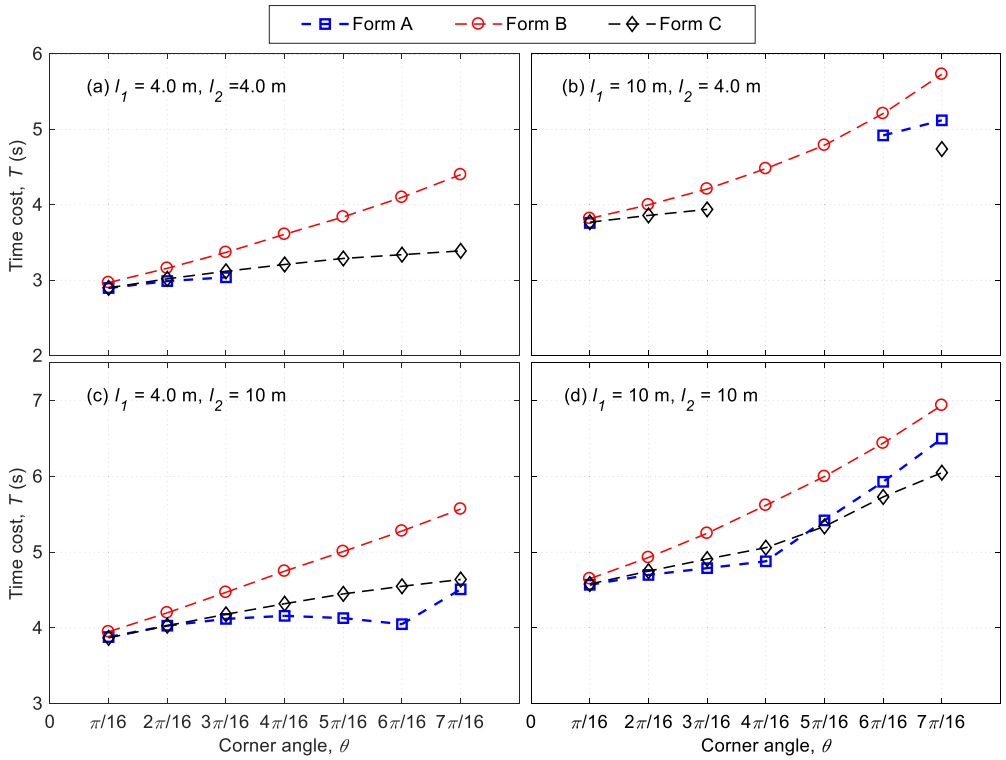

FIGURE 25. Least-time cost comparison of forms A, B, and C with $D = 2.0$ m.

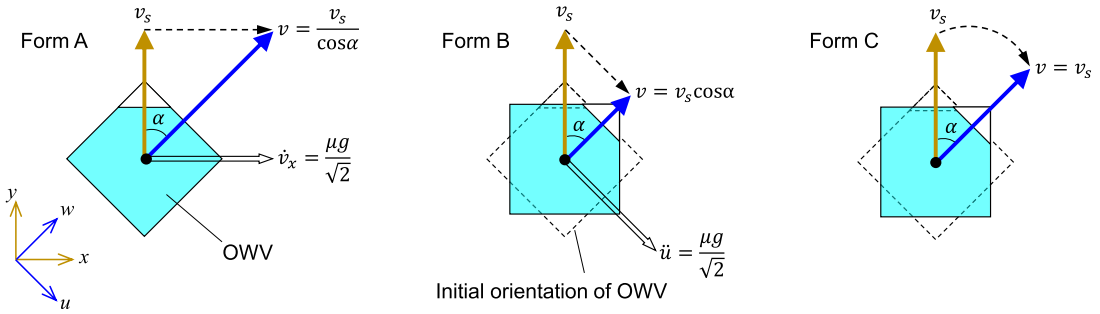

FIGURE 26. Velocity variation of OWV before point P.

again because the vehicle has to switch from pattern A0 to another pattern to avoid path deviation.

As shown in Fig. 25(d), when both l_1 and l_2 are large, the difference in the time cost between forms A and C varies according to θ. Form A costs less time than form C for $\theta \leq 4\pi/16$, while the converse is true for $\theta > 4\pi/16$. When θ is relatively small, form A does not require deceleration to travel without deviation. In this case, the velocity becomes larger than the velocity at point S, as explained in Fig. 26. However, the velocity of form C during the turning motion remains unchanged. Then, form A is advantageous. When θ is larger than $4\pi/16$ with form A, the OWV must decelerate before turning to avoid deviation even if l_2 is large. In contrast, form C can achieve the largest driving force in the second linear motion because the adjustment of the orientation is finished during turning. Then, form C is superior to form A.

Next, we discuss the effect of the variation of the path width D. Fig. 27 shows the time cost variation of all forms when D varies with $\theta = 3\pi/16$ and $6\pi/16$. With regards to D, form B costs more time than forms A and C. The difference between them is small when D is relatively small but becomes larger when D increases. The reason is thought to be the same as that described in the discussion of Fig. 26. In form B, the time cost slightly increases when D becomes large because the quickest pattern changes from B1 to B0 due to the deviation of B1, as explained in section 4.2.

Forms A and C show the same tendency and their difference is small in Fig. 27. When θ is small, form A costs less time than form C, as shown in Fig. 27(a), which is the same as in Fig. 25. However, when θ is large, form C can compete with form A under some conditions, as shown in Fig. 27(b). Although form A costs less time than form C when D is sufficiently small, that is, $D \leq 0.8$ m, form C surpasses form

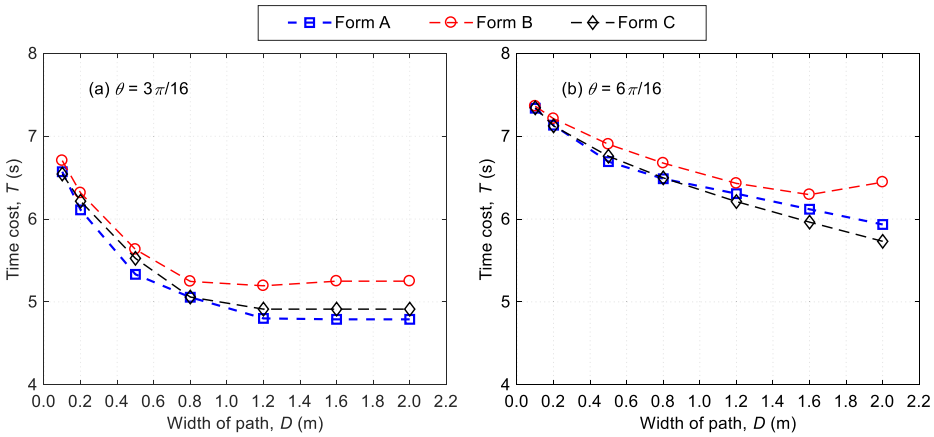

FIGURE 27. Least-time cost comparison of three forms with $l_1 = l_2 = 10$ m.

A when D becomes larger. This is because form C, in which the vehicle finishes the rotation during turning, can apply the maximum acceleration for the entirety of the second linear motion. In other words, the vehicle can converge with the centerline sooner in form C than in form A, after which the vehicle can use the driving force for acceleration to complete the trajectory.

In summary, the results suggest that the optimum strategy is to travel by form A or C instead of form B unless deviation occurs because form B costs more time and the difference between forms A and C is small. Strictly speaking, although their performance is generally similar, form C is advantageous when both θ and D are large and l_1 is equal to or larger than l_2, while form A is advantageous in other cases.

V. CONCLUSION

Vehicles are widely used for transporting products in factories and warehouses. Vehicles equipped with omnidirectional wheels can move in any direction, they make efficient motion possible even in a narrow passage. Therefore, there are many possible traveling strategies for an omnidirectional wheeled vehicle to pass through an angled passageway or corner. However, what strategy is suitable for what situations has not been fully explored. With that point in mind, this study constructed a numerical model of a vehicle with four omni wheels and then simulated and compared three driving strategies in terms of the time cost of traveling a designated path with one corner. This study obtained the following results:

1) Three traveling strategies for an OWV were proposed based on their kinetic models by considering the order of rotation and turning: form A, rotation after turning; form B, rotation before turning; and form C, rotation during turning. The possible time-optimal patterns of these traveling strategies were discussed theoretically based on the magnitude of acceleration and the necessity of deceleration.
2) The motion patterns of each traveling strategies were analyzed when the traveling area conditions, including the corner angle, path width, and path length, were varied. The time cost is the smallest when the vehicle can run without deceleration before turning (A0, B0, and C0), which is possible when the path is wide and the corner angle is small. When both the path width and angle are small, the pattern in which the vehicle turns with a large radius (A2, B2, and C2) is optimal because it maintains the highest possible velocity during turning. When the corner angle is large and the path length before the corner is larger than that after the corner, the pattern with the lowest time cost switches to the one in which the vehicle turns with a small radius by decelerating before turning (A3, B1, and C1).
3) The time cost of the three traveling strategies was compared to find out which strategy was suitable for each situation. It is advantageous for the vehicle to travel by form A when the corner angle or the path width is small. When both of them become larger, form C costs less time than the other forms. Form B is advantageous when the path length after the corner is small, where the vehicle cannot finish the traveling path by forms A and C. Overall, form A or C is a better driving strategy than form B for passing through a corner.

Based on the features of these driving strategies, we plan to design a time-optimal controller by referring to the model predictive approach in future work.

REFERENCES

[1] M. J. A. Safar, "Holonomic and omnidirectional locomotion systems for wheeled mobile robots: A review," *Jurnal Teknologi*, vol. 77, no. 28, pp. 91–97, Dec. 2015, doi: 10.11113/jt.v77.6799.
[2] K. Tadakuma, "Omnidirectional mobile and driving mechanism," *J. Robot. Soc. Jpn.*, vol. 29, no. 6, pp. 516–519, 2011, doi: 10.7210/jrsj.29.516.
[3] A. V. Borisov, A. A. Kilin, and I. S. Mamaev, "Dynamics and control of an omniwheel vehicle," *Reg. Chaotic Dyn.*, vol. 20, no. 2, pp. 153–172, May 2015, doi: 10.1134/S1560354715020045.
[4] S. K. Saha, J. Angeles, and J. Darcovich, "The design of kinematically isotropic rolling robots with omnidirectional wheels," *Mech. Mach. Theory*, vol. 30, no. 8, pp. 1127–1137, Nov. 1995, doi: 10.1016/0094-114X(95)00042-W.

[5] V. A. Joshi, R. N. Banavar, and R. Hippalgaonkar, "Design and analysis of a spherical mobile robot," *Mechanism Mach. Theory*, vol. 45, no. 2, pp. 130–136, Feb. 2010, doi: 10.1016/j.mechmachtheory.2009.04.003.
[6] J. C. L. Barreto S., A. G. S. Conceicao, C. E. T. Dorea, L. Martinez, and E. R. de Pieri, "Design and implementation of model-predictive control with friction compensation on an omnidirectional mobile robot," *IEEE/ASME Trans. Mechatronics*, vol. 19, no. 2, pp. 467–476, Apr. 2014, doi: 10.1109/TMECH.2013.2243161.
[7] A. A. Zobova and Y. V. Tatarinov, "The dynamics of an omni-mobile vehicle," *J. Appl. Math. Mech.*, vol. 73, no. 1, pp. 8–15, May 2009, doi: 10.1016/j.jappmathmech.2009.03.013.
[8] M. Komori, K. Matsuda, T. Terakawa, F. Takeoka, H. Nishihara, and H. Ohashi, "Active omni wheel capable of active motion in arbitrary direction and omnidirectional vehicle," *J. Adv. Mech. Design, Syst., Manuf.*, vol. 10, no. 6, 2016, Art. no. JAMDSM0086, doi: 10.1299/jamdsm.2016jamdsm0086.
[9] M. Komori and K. Matsuda, "Velocity characteristics of active omni wheel considering transmitting mechanism," in *Proc. EuCoMeS*, Aachen, Germany, 2018, pp. 109–116, doi: 10.1007/978-3-319-98020-1_13.
[10] T. Terakawa, M. Komori, Y. Yamaguchi, and Y. Nishida, "Active omni wheel possessing seamless periphery and omnidirectional vehicle using it," *Precis. Eng.*, vol. 56, pp. 466–475, Mar. 2019, doi: 10.1016/j.precisioneng.2019.02.003.
[11] A. Gfrerrer, "Geometry and kinematics of the mecanum wheel," *Comput. Aided Geometric Des.*, vol. 25, no. 9, pp. 784–791, Dec. 2008, doi: 10.1016/j.cagd.2008.07.008.
[12] Y. Li, S. Dai, Y. Zheng, F. Tian, and X. Yan, "Modeling and kinematics simulation of a mecanum wheel platform in RecurDyn," *J. Robot.*, vol. 2018, pp. 1–7, Jan. 2018, doi: 10.1155/2018/9373580.
[13] J. E. Mohd Salih, M. Rizon, and S. Yaacob, "Designing omni-directional mobile robot with mecanum wheel," *Amer. J. Appl. Sci.*, vol. 3, no. 5, pp. 1831–1835, May 2006, doi: 10.3844/ajassp.2006.1831.1835.
[14] W.-H. Chen, C.-P. Chen, J.-S. Tsai, J. Yang, and P.-C. Lin, "Design and implementation of a ball-driven omnidirectional spherical robot," *Mechanism Mach. Theory*, vol. 68, pp. 35–48, Oct. 2013, doi: 10.1016/j.mechmachtheory.2013.04.012.
[15] A. Weiss, R. G. Langlois, and M. J. D. Hayes, "The effects of dual row omnidirectional wheels on the kinematics of the Atlas spherical motion platform," *Mechanism Mach. Theory*, vol. 44, no. 2, pp. 349–358, Feb. 2009, doi: 10.1016/j.mechmachtheory.2008.03.013.
[16] Q. Zhan, Y. Cai, and C. Yan, "Design, analysis and experiments of an omni-directional spherical robot," in *Proc. IEEE Int. Conf. Robot. Autom.*, May 2011, pp. 4921–4926, doi: 10.1109/ICRA.2011.5980491.
[17] T. Kalmár-Nagy, "Real-time trajectory generation for omni-directional vehicles by constrained dynamic inversion," *Mechatronics*, vol. 35, pp. 44–53, May 2016, doi: 10.1016/j.mechatronics.2015.12.004.
[18] C.-C. Tsai, C.-Z. Kuo, C.-C. Chan, and X.-C. Wang, "Global path planning and navigation of an omnidirectional Mecanum mobile robot," in *Proc. CACS Int. Autom. Control Conf. (CACS)*, Dec. 2013, pp. 85–90, doi: 10.1109/CACS.2013.6734112.
[19] R. L. Williams and J. Wu, "Dynamic obstacle avoidance for an omnidirectional mobile robot," *J. Robot.*, vol. 2010, pp. 1–14, Sep. 2010, doi: 10.1155/2010/901365.
[20] M. Abe, "Body roll and vehicle dynamics," in *Automotive Vehicle Dynamics Theory and Applications*, vol. 1, 2nd ed, Japan: Tokyo Denki Univ. Press, 2012, ch. 6, sec. 6, pp. 165–177.

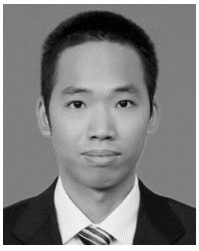

SIYING LONG received the B.E. degree in logistics engineering from the Wuhan University of Technology, Wuhan, China, in 2008, and the M.E. degree in mechanical design and theory from Zhejiang University, Hangzhou, China, in 2014. He is currently pursuing the Ph.D. degree with the Department of Mechanical Engineering and Science, Graduate School of Engineering, Kyoto University. His current research interest is mobile robots.

TATSURO TERAKAWA received the B.E. degree in mechanical engineering from Kyoto University, Japan, in 2014, and the M.E. and Dr.Eng. degrees from the Department of Mechanical Engineering and Science, Graduate School of Engineering, Kyoto University, in 2016 and 2019, respectively.

Since 2019, he has been an Assistant Professor with the Department of Mechanical Engineering and Science, Kyoto University. His research in Kyoto University is focused on mechanisms and control of wheeled mobile robots, actuator mechanisms, and design.

Dr. Terakawa is a member of JSME and JSDE. He received a JSME Medal for Outstanding Paper, in 2018, a JSME Miura award, in 2016, a JSDE encouragement award, in 2018, an IFToMM World Congress Best Application Paper Award, in 2019, a JSME MD&T division encouragement presentation, in 2016, an FA Foundation paper award, in 2019, and JSAE graduate school research encouragement awards, in 2016 and 2019.

MASAHARU KOMORI (Member, IEEE) received the B.E. degree in precision engineering from Kyoto University, in 1995, the M.E. degree from the Graduate School of Kyoto University, in 1997, and the Ph.D. degree in engineering from Kyoto University, in 2002.

From 1999 to 2000, he was a student in the doctoral course in Kyoto University, and in 2000, he became a Research Assistant at the Graduate School of Engineering, Kyoto University. In 2004, he became an Associate Professor at Kyoto University. In 2017, he became a Professor at Kyoto University and currently belongs to the Department of Mechanical Engineering and Science, Kyoto University. His research interests include riding robotics, vehicles, robots, operation, transmission, gear, and measurement.

Dr. Komori is a fellow of the Japan Society of Mechanical Engineers (JSME) and a member of the Robotics Society of Japan (RSJ), Japan Society of Design Engineering (JSDE), and Japan Society for Precision Engineering (JSPE). He was a recipient of The Young Scientists' Prize of The Commendation for Science and Technology by the Minister of Education, Culture, Sports, Science and Technology, in 2011, a WT award, in 2013, three JSME medals for outstanding paper, in 2009, 2013, and 2018, a JSME medal for new technology, in 2014, a JSME young engineers award, in 2005, a best paper award from JSDE, in 2012, an Eiji Mutoh excellent design award, in 2012, an FA Foundation paper award, in 2014, and a Nagamori award, in 2017. His paper was selected as one of the best articles published in measurement science and technology, in 2009.

TAKUMI OUGINO received the B.E. degree in mechanical engineering from Kyoto University, Japan, in 2018, and the M.E. degree from the Department of Mechanical Engineering and Science, Graduate School of Engineering, Kyoto University, in 2020. His research in Kyoto University was on mobile robots.